Electronic interaction of slow hydrogen, helium, nitrogen, and neon ions with silicon

Eleni Ntemou [1,*] Svenja Lohmann [1,2] Radek Holeňák [1] and Daniel Primetzhofer [1]

[1]*Department of Physics and Astronomy, Uppsala University, 751 20 Uppsala, Sweden*

[2]*Institute of Ion Beam Physics and Materials Research, Helmholtz-Zentrum Dresden-Rossendorf e.V. (HZDR), 01328 Dresden, Germany*

(Received 22 February 2023; revised 5 April 2023; accepted 10 April 2023; published 26 April 2023)

We investigate the electronic excitation of silicon by hydrogen, helium, nitrogen, and neon ions for ion energies ranging from several tens to a few hundred kiloelectronvolts. Experiments are carried out in transmission geometry using a time-of-flight medium energy ion scattering system. The targets are self-supporting, single-crystalline Si (100) foils with nominal thicknesses of 50 and 200 nm. Stopping cross-sections (SCSs) are derived and compared with datasets available from the literature and predictions from theory. The results for H projectiles reveal good agreement with literature datasets, within quoted uncertainties. For He projectiles, the results show good agreement with most of the literature data. For N ions, higher values than reported in the literature are measured. For Ne, where literature data are scarce, we extend the velocity regime for which data exist by a factor of two toward higher velocities. The electronic SCS is found to be proportional to ion velocity for all impinging ions, for velocities below the Bohr velocity ($v < v_0$). Comparison with theoretical predictions for a homogeneous free electron gas indicates strong contributions of local energy loss processes different from those expected for electron-hole pair excitation in binary collisions for all ions different from protons.

DOI: 10.1103/PhysRevB.107.155145

I. INTRODUCTION

The energy dissipation of energetic charged heavy particles traversing through matter has been the subject of numerous experimental and theoretical studies for many decades [1]. This interest stems from the importance of a qualitative and quantitative understanding of the interaction between ions and solids for different fields in fundamental physics as well as in applied science and technology. To enable and maintain state-of-the-art materials characterization and modification techniques based on energetic ions, e.g., ion beam analysis, ion implantation, irradiation, sputtering, or hadron therapy, accurate knowledge of the energy loss per path length is a prerequisite. Silicon (Si) is one of the most implemented materials in the semiconductor industry, omnipresent in electronic and optical devices. Thus, extending data on electronic energy loss in the literature for N and Ne in Si toward lower energies and enriching the already existing datasets for He and H projectiles by data recorded in a time-of-flight transmission approach is highly relevant.

The mean energy loss per unit path length dE/dx of an impinging ion is defined as the stopping power S and is usually employed to quantify the energy loss. A related quantity, independent of the potentially unknown target density, is the stopping cross-section (SCS), which corresponds to the stopping power normalized by the atomic volume density. The mechanisms of energy loss of ions at all but the highest energies are inelastic Coulomb interactions with the atomic electrons, namely, electron excitation and ionization, inducing what is referred to as electronic stopping power (S_e), and elastic collisions with the atomic nuclei of the target material which are the basis for the nuclear stopping power (S_n) of the material for the impinging particle. The total stopping power is the sum of S_e and $S_n (S = S_e + S_n)$. The atomic number of ions and target nuclei as well as the ion velocity determine the relative contributions of the electronic and nuclear stopping to the total energy loss.

For higher velocities which correspond to the right side of the observed characteristic maximum in the stopping power, which is commonly denoted as the Bragg peak [2], energy dissipation mechanisms are well understood: The interactions are adiabatic, and the predominantly electronic stopping is well predicted by first-principles theories [3,4]. In the low-velocity regime (around and below the Bohr velocity v_0), the ion velocity is comparable with the velocity of valence and conduction electrons, and the interaction obtains a more dynamic character. In this regime, the nuclear stopping power also becomes significant, mainly for heavier impinging ions. A successful model for describing ion-electron interactions in this regime is the treatment of the valence electrons as a free electron gas (FEG) [5,6]. This model predicts that the stopping power is proportional to velocity $S = Q(Z_1, r_s)v$, where Q corresponds to the friction coefficient of the FEG. Here, Q is a function of the atomic number of the ion Z_1 and the Wigner-Seitz radius of the sphere containing one electron, the so-called density parameter of the FEG (r_s). In the context of the FEG model, the only possible energy dissipation mechanisms are electron-hole pair excitation in binary collisions as well as plasmon excitations. The latter, however, are not

*eleni.ntemou@physics.uu.se

expected at energies of only a few tens of kiloelectronvolts [7,8].

Experimentally, in the velocity regime investigated here, deviations from velocity proportionality of the SCS have been found for both protons [9] and heavier ions [10]. For protons, a clear velocity proportionality was observed for, e.g., Al, Sb, and Bi [9], while late transition metals exhibited clear deviations which could be successfully explained by the change in effective density within a FEG for materials with excitation thresholds for d electrons, i.e., Au and Cu [10]. For early transition and rare-earth metals, however, high electronic SCSs for protons were found drastically exceeding predictions based on the number of available conduction electrons, an effective breakdown of the FEG model [11]. Very recently, different advanced time-dependent approaches have been employed to model electronic excitations more accurately, showing clear nonlinearities also for specific early transition metals [12] and including inner shell effects [13–15].

Deviations from velocity proportionality in the low-velocity regime have also been observed for insulators like LiF, where a velocity threshold exists below which ions move without transferring energy to the electronic system [16], however at energies much lower than predicted from static theory [5,17]. Time-dependent approaches could yield better agreement [18], but quantitative predictions are not available on a broad basis.

Additionally, for ions heavier than protons, charge exchange and electron promotion effects have been claimed to effectively contribute to the energy loss [19–21]. These effects show a clear impact parameter dependence [22,23], in accordance with differences in the specific inelastic energy loss of low-energy ions transmitted through single-crystalline targets in different orientations [24–26]. Again, recently, time-dependent modeling [27] has led to an improved agreement for specific ion-projectile combinations [25].

Accordingly, dynamic processes in the interaction, such as charge exchange and electron promotion processes are theoretically expected to contribute to the electronic stopping in random sample orientation or for polycrystalline targets. Such impact-parameter-dependent processes could result in differences between energy loss measurements in transmission geometries, where transmitted particles only undergo collisions with comparatively large impact parameters, and measurements in backscattering geometries, where at least one small impact parameter collision (large angle scattering) is necessary. For energies of several tens of kiloelectronvolts, no pronounced effect of the experimental geometry on the electronic stopping power was observed for random orientation of the material in both backscattering and transmission geometry [28]. For very low velocities, significant effects of the experimental geometry have been predicted [29], which are, however, not linked to multielectron excitation processes.

In this paper, we study the electronic stopping power of Si for both light and heavy ions, and we analyze the data considering the abovementioned understanding while providing further reference data for benchmarking advanced computational approaches. We perform an analysis of the magnitude of electronic stopping, with respect to predictions from density functional theory (DFT), with respect to the modeling software DPASS [30–32] and ESPNN [33,34] and in comparison to aluminum, as a nearby element, for which both excellent agreement with theoretical predictions—for protons—and pronounced deviations from expectations for a FEG—for helium—have been found.

A. Experimental setup

We performed experiments using the time-of-flight medium energy ion scattering system at the 350-keV Danfysik Implanter at Uppsala University [35,36]. Pulsed beams of singly positively charged H, H_2, He, N, and Ne ions with energies 11–300 keV were transmitted through single-crystalline, self-supporting Si (100) membranes aligned in random orientation (namely, the rotation angles were at least $R_x = 5^\circ$ around the x axis and $R_y = 10^\circ$ around the y axis with respect to the channeling orientation) to obtain trajectories with a broad, stochastic distribution of impact parameters. The pulsing of the ion beams was achieved through electrostatic chopping combined with a vertical gating pulse and four sets of slits located along the beamline. The resulting beam spot was $< 1\times1\,\mathrm{mm}^2$, and the time resolution was $\sim$ 1–7 ns, corresponding to an energy resolution of 0.7–3 keV for light ions and 2–6 keV for heavier ions (N and Ne). Both position and time-of-flight information for the transmitted particles were obtained from a large solid angle (0.13 sr), position-sensitive microchannel plate detector [37]. Particles are detected irrespective of their charge, and due to effective kinetic electron emission at the detected ion velocities [38], no significant charge-state-dependent sensitivity is assumed. The position information was acquired by a set of delay lines. The repetition rate of the impinging pulses at the detector was kept $<$ 13 kHz, resulting in an effective current below a few femtoampere and typically at most a single ion per pulse. The detector is located 290 mm behind the target and has a diameter of 120 mm, which corresponds to an angular radius of 11.5°. The Si samples were mounted on the sample holder located in the center of the scattering chamber and were aligned with a 6-axis goniometer. During all experiments, the pressure in the scattering chamber was kept $< 2\times10^{-8}$ mbar.

The samples were self-supporting, single-crystalline Si (100) membranes (Norcada Inc. [39]) with nominal thicknesses of 50 and 200 nm. The sample thicknesses were confirmed by means of Rutherford backscattering spectrometry (RBS) using 2-MeV He^+ ions. The RBS experiments were performed at the 5-MV 15SDH-2 Pelletron Tandem accelerator at Uppsala University and are described in detail in Ref. [25]. The obtained thickness values were 200 nm with a relative uncertainty better than 6% and 53 nm with a relative uncertainty of 7.5%. The sample was dipped in a hydrofluoric (HF) acid solution prior to the measurements with N and Ne projectiles and the low-energy measurements with He.

The recorded two-dimensional intensity distribution for He ions with primary energy of 22 keV transmitted through the 50-nm Si (100) self-supporting foil is shown in Fig. 1. The membrane was rotated 5° around the x axis and 10° around the y axis with respect to the alignment of the beam with the ⟨100⟩ crystal axis. The beam was not aligned with any crystal axis or plane of the Si (100) membrane, resulting in a (pseudo)random geometry. In this random orientation, most of the ions exit the crystal close to the direction of the impinging

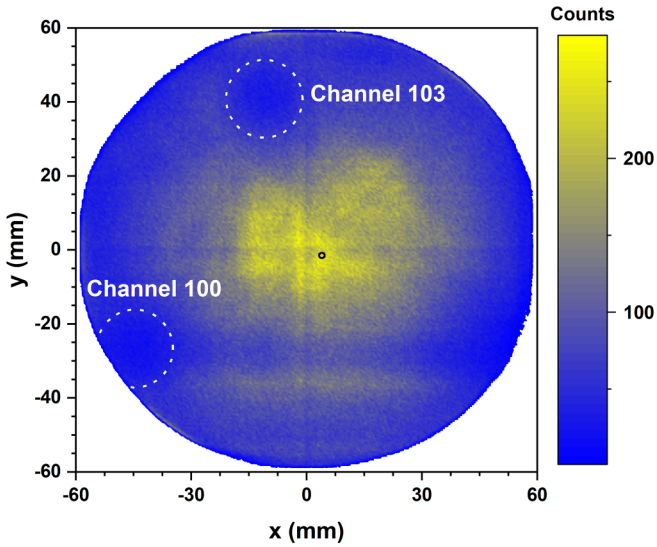

FIG. 1. Two-dimensional intensity distribution of He^+ ions with 22 keV primary energy transmitted through a 53-nm Si (100) self-supporting foil. The membrane is turned by $R_x = 5°$ around the x axis and by $R_y = 10°$ around the y axis with respect to the (100) axis to obtain random trajectories. The black circle indicates the region from which trajectories were considered for evaluation, while the white dotted circles indicate the position of the (100) and (103) channels. The faded cross visible in the center of the map is an artifact from the Cobold PC software; nonetheless, it does not affect the analysis of the trajectories.

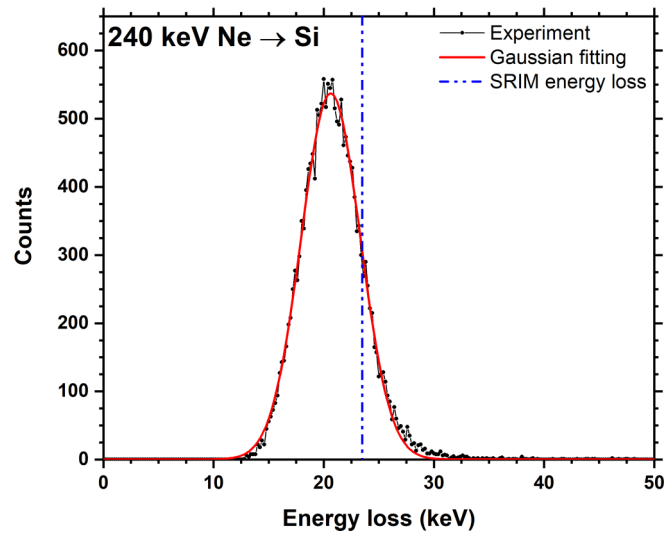

FIG. 2. Energy loss spectrum of 240 keV Ne^+ transmitted through a 50-nm Si (100) self-supporting foil. Data are taken from a circular region of interest with 1-mm radius, corresponding to transmission with minimum deflection. The vertical blue dotted line is the energy loss predicted for amorphous Si by SRIM [40], while the red line corresponds to a Gaussian distribution fitted to the energy loss peak.

beam. In Fig. 1, the observed intensity distribution also shows the blocking effects originating from channels 100 and 103 and the 110 plane.

B. Data analysis

For the evaluation of the energy loss by converting the time-of-flight spectra to energy spectra, the acquisition software Cobold PC [37] was used. The energy spectra were generated by selecting only trajectories ending in a limited region of the detector, a small circular region of interest around the initial beam position with a radius of 1 mm (corresponding to scattering angles of $\pm 0.2°$), visible in Fig. 1. An exemplary energy loss spectrum derived for Ne ions with primary energy 240 keV is shown in Fig. 2, along with a Gaussian fit to the energy loss peak. As shown in Fig. 2, the Gaussian distribution describes the peak adequately, although a tail at the high energy loss side can be observed. Nonetheless, the position of the centroid of the peak remains unaffected by this asymmetry, which is attributed to a minor contribution from nuclear energy loss, which is more pronounced at lower energies, as well as to electronic losses acquired by a few large energy loss events [41]. Hence, the energy loss is determined via the centroid value of the Gaussian fitting at the corresponding peak, visible in Fig. 1. The measured energy loss corresponds almost exclusively to the electronic energy loss for the light projectiles and the higher impinging energies. However, for the lower energies and heavier projectiles, the contribution of nuclear energy loss to the total energy loss must be considered. For the estimation and subtraction of the nuclear energy loss contribution, Monte Carlo simulations of our transmission experiments were employed using the TRBS simulation code [42]. For all simulations, we used the universal stopping power model, the universal screening model, and the universal scattering potential [43]. For each energy and ion, we performed two simulations: one with the screening correction factor set to 1, simulating the experimental conditions, and one with the screening factor set to 0.001, simulating an imaginary condition where the Coulomb potential does not affect the ion trajectory, thus leading to only electronic contribution to the total energy loss. By comparing and subtracting the two distributions of the exiting ions at angles between 0° and 1°, the contribution of the nuclear energy loss can be estimated. We subtracted nuclear contributions for ion velocities up to $\sim 0.5\, v/v_0$. The contribution for H and He projectiles was $< 3\%$ at all energies, while for N and Ne projectiles, it was $< 6\%$ at all energies.

For He, N, and Ne projectiles, the electronic SCS was calculated from the measured energy loss by considering the thickness of the Si target and the gradual change in ion energy. To consider this gradual change, we employed a numerical integration procedure, described in detail in Ref. [26]. The numerical integration procedure was performed iteratively until agreement between the measured and the calculated energy loss values was achieved.

For H projectiles, the studied primary energy values are around the stopping maximum; thus, the velocity dependence of the stopping is not straightforward. We, therefore, used the TRBS code to determine the electronic stopping power, as TRBS allows us to modify electronic stopping by a simple multiplicative factor. We simulated the experiment, tuning the electronic stopping power until a good fit to the experimental data was achieved. The simulations were run employing the Thomas-Fermi-Molière potential [44] with uncorrected screening. However, since the energy deposition of protons

in this velocity regime is practically fully electronic, specific choices of the scattering potential or screening corrections are not expected to impact the result.

II. RESULTS AND DISCUSSION

In Figs. 3–6, the experimentally deduced SCS values are presented for H, He, N, and Ne ions, respectively, as a function of the ion velocity, in atomic units (v/v_0). The error bars in the presented datasets include the statistical uncertainties originating from the peak fitting, potential systematic uncertainties in distance between sample and detector, the time resolution, and the systematic uncertainty of target thickness obtained from RBS.

In Fig. 3, for H projectiles, the present data agree with the previously measured datasets from Tran *et al.* [45], Brocklebank *et al.* [46], Ikeda *et al.* [47], Konac *et al.* [48], and Hobler *et al.* [49] within quoted uncertainties. All these datasets were obtained in backscattering geometry, except that from Hobler *et al.* [49], where the electronic SCS values were obtained combining ion implantation and SIMS. The datasets by Famá *et al.* [50] and Niemann *et al.* [51] display somewhat lower values at the stopping maximum and for lower velocities. Good agreement is found with predictions from SRIM [40], DPASS (v. 2.11—database version 21.06—default settings [32]), PSTAR [53], which uses single collisions with the lattice atoms to calculate the specific energy loss, and ESPNN [34], which trains a deep neural network to accurately reproduce all the available experimental values and predict new results.

In Fig. 4, for He projectiles, good agreement with the previously measured data by Pearce and Hart [54], measured in backscattering geometry using thick targets, and the medium

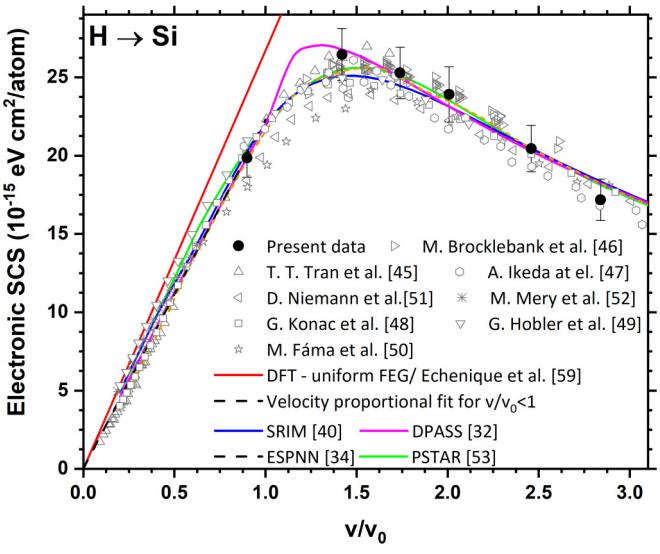

FIG. 3. Electronic stopping cross-sections (SCSs) of Si for H ions (H_2^+ for the data point at the lowest velocity) as a function of velocity. SRIM (blue line) and ESPNN predictions (dark yellow dashed line) along with theoretical predictions and previously measured datasets are also included [44–50,52,67]. The black dashed line corresponds to a velocity proportional fit to the present SCS (up to $1 v/v_0$) as a function of velocity.

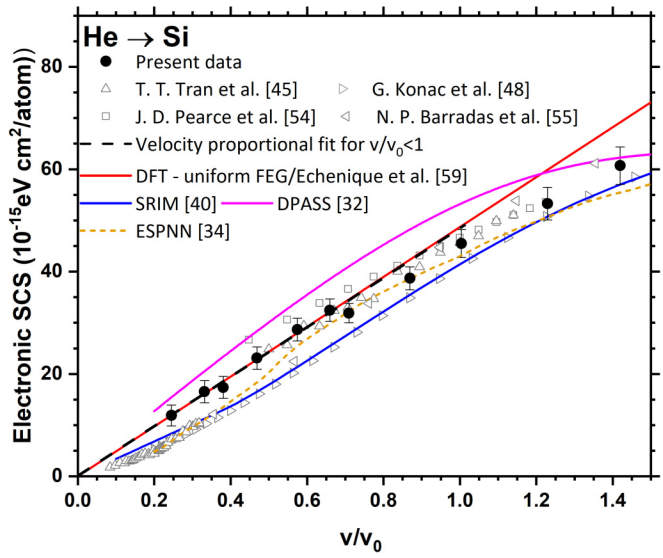

FIG. 4. Electronic stopping cross-sections (SCSs) of Si for He ions as a function of velocity. SRIM (blue line) and ESPNN predictions (dark yellow dashed line) along with theoretical predictions and previously measured datasets are also included. The black dashed line corresponds to a velocity proportional fit to the present SCS (up to $1\ v/v_0$) as a function of velocity.

energy ion scattering backscattering data by Tran *et al.* [45] is observed. However, the low-energy data by Tran *et al.* [45], measured using a relative measurement technique by employing Al reference foils in backscattering geometry [45], and the data by Konac *et al.* [48], also measured in backscattering geometry with subtraction of the nuclear energy loss by using literature data, display lower values. Agreement within the quoted uncertainties is observed with the dataset by Barradas *et al.* [55] for the high-velocity regime, whereas for lower velocities, the present dataset obtained in transmission displays higher values than datasets obtained in backscattering from thin films in accordance with predictions by Schinner *et al.* [29]. Data by Pearce and Hart [54] extrapolating to even higher values at low energies was measured by yet another approach, analyzing the energy-dependent intensity of a bulk target. Predictions from ESPNN and SRIM also underestimate the electronic SCS values. The long-dashed line in Fig. 3 and 4 indicates a velocity-proportional SCS fitted to the present data for $v/v_0 < 1$. The prediction from DPASS indicates higher stopping values than the present experimental data. This deviation is attributed to the fact that DPASS determines the energy loss at the mean charge instead of the mean value of the charge-dependent energy loss. As mentioned in Ref. [31], this description involving a mean charge state becomes questionable for the case of He.

In Fig. 5, for N projectiles, the present data display higher values than the scarce previously measured data from Santry and Werner [56] and Grahmann and Kalbitzer [57]. The data point from Hoffman *et al.* [58] agrees with the presented values. The data by Grahmann and Kalbitzer [57] were derived in an indirect approach, by irradiating a tilted (to avoid channeling) Si detector with ion beams and extracting both electronic and nuclear stopping by accounting for the total

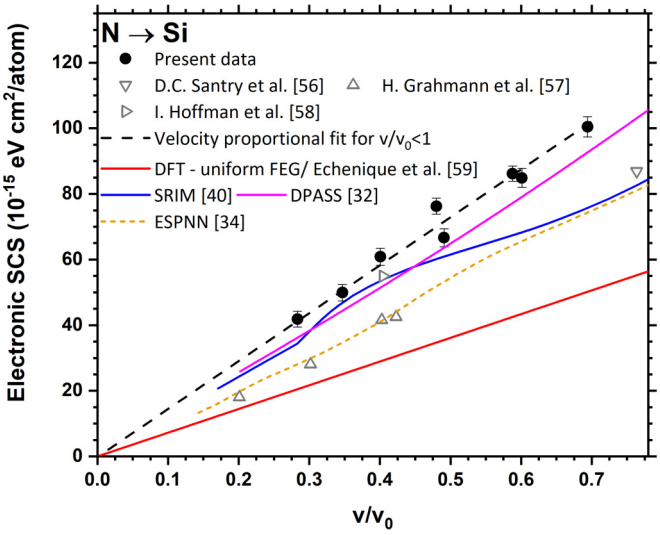

FIG. 5. Electronic stopping cross-sections (SCSs) of Si for N ions as a function of velocity. SRIM (blue line) and ESPNN predictions (dark yellow dashed line) along with theoretical predictions and previously measured datasets are also included. The black dashed line corresponds to a velocity proportional fit to the present SCS (up to 1 v/v_0) as a function of velocity.

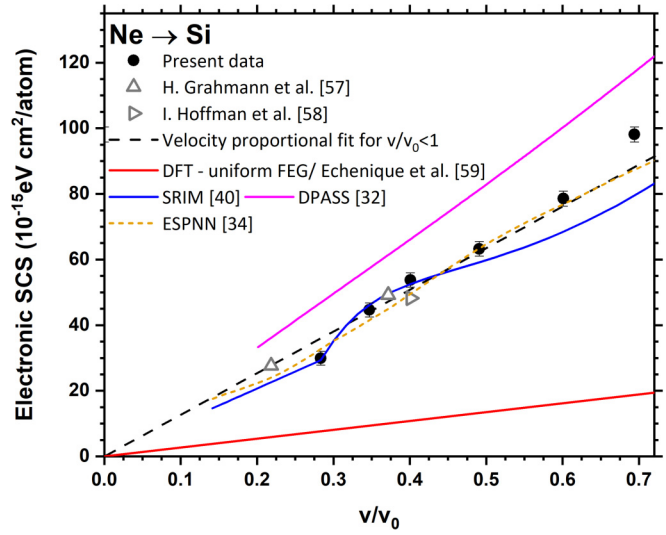

FIG. 6. Electronic stopping cross-sections (SCSs) of Si for Ne ions as a function of velocity. SRIM (blue line) and ESPNN predictions (dark yellow dashed line) along with theoretical predictions and previously measured datasets are also included. The black dashed line corresponds to a linear fit to the present SCS (up to 1 v/v_0) as a function of velocity.

energy deposition using the ionization yield. The predictions by SRIM and ESPNN display lower values. Predictions from DPASS were found systematically lower by $\sim 15\%$ than our data.

In Fig. 6, for Ne projectiles, the present data for lower velocities agree with the data by Grahmann and Kalbitzer [57] and Hoffman *et al.* [58] as well as with SRIM and ESPNN predictions. For higher velocities, the present data indicate higher values than the ones predicted by SRIM. In the case of Ne projectiles, where literature data are scarce, our data extend the range of velocities for which data is available by a factor of ~ 2 toward higher values. DPASS predicts systematically $\sim 20\%$ higher values. In the cases of He and Ne ions, the present data lie below the DPASS curves. For both N and Ne ions, for the lowest investigated velocities ($v/v_0 < 1$), the electronic SCS shows a linear velocity dependence, as displayed by the dashed lines in Figs. 5 and 6.

In Figs. 3–6, the deduced values are additionally compared with nonlinear DFT calculations for a homogeneous FEG according to the model by Echenique *et al.* [59]. The employed density parameter $r_s = 1.97$ for a FEG was obtained from the experimental plasmon energy of Si [60,61]. On this basis, the friction coefficient Q for protons and for $r_s = 1.97$ was calculated using curve D of Fig. 12 in Ref. [59]. As shown in Fig. 3, the DFT model predicts a higher friction coefficient Q than featured by the present data. This observation can be qualitatively understood since ~ 4 electrons per Si molecule effectively contribute to the FEG (calculated using Eq. (6) in Ref. [60]), which agrees with the expectations from the available electronic states; however, Si is a semiconductor with a small band gap of 1 eV, which limits the excitations compared with a FEG with the same number of electrons. For He ions, the friction coefficient was calculated by using the DFT results for He ions (curve E of Fig. 12 in Ref. [59]). Predictions are found to agree with the present values for low velocities. However, employing the effective electron density as obtained from a fit of the friction coefficient to the data for protons to predict electronic SCSs for He in Si leads to values lower than the experimentally measured ones. The different response of Si to excitation by protons and helium ions, expressed by a relative excess in electronic stopping for He in comparison with DFT-predictions for He, can be explained on a similar basis as what has been earlier suggested for aluminum [19]: as silicon features similar energy thresholds as aluminum for charge exchange in low-energy ion scattering ($E < 500$ eV [62]), the apparent and unphysical increase in r_s in comparison with protons can be reasoned by contributions different from direct electron-hole pair excitations as well as an accordingly altered mean charge state [24].

A linear fit to the present stopping data for H ions leads to a density parameter $r_s = 2.5$, by using the DFT stopping as a function of the density parameter curve from Ref. [59]. With this density parameter value, one could calculate the plasmon energy to be $\hbar\omega_p = 11.92$ eV and compare it with the value that corresponds to $r_s = 1.97$ (literature value from plasmon energies), which is $\hbar\omega_p = 16.6$ eV [60].

For N and Ne ions, DFT predictions were extracted using the expression for the effective charge from Ref. [59]:

$Z_1^* = [\frac{dE/dx(Z_1)}{dE/dx(Z_1=1)}]^{1/2}$. For each Z_1, first, we calculated the corresponding Z_1^* for $r_s = 1.97$ based on Fig. 15 in Ref. [59] by performing linear interpolation between the values $r_s =$ 1.5 and 2, and subsequently, we calculated the friction coefficient by using the friction coefficient as obtained for protons from the linear fit to our presented data. For both heavier ions, DFT for a uniform FEG significantly underestimates the SCS. This observation could be attributed to the fact that an additional mechanism, different from electron-hole pair excitation in binary collisions, severely contributes to energy deposition in the electronic system. Processes contributing to the energy loss could be electron promotion including formation of

molecular orbitals [63] for short interaction distances and the significant altering of the mean charge state by ionization of the projectile, leading to increased specific energy loss along the trajectories. Another possible contribution is the higher electron density encountered by the ions in close collisions.

One can, in an inverse approach, also calculate how the effective density, which is necessary to describe the present data in the framework of excitation of a FEG, is changing for different projectiles. The effective density is calculated by linear extrapolation of predictions for the effective charge as a function of the density parameter, as shown in Ref. [54]. The measured friction coefficient for N corresponds to a FEG with a density parameter of $r_{s,\mathrm{exp}} = 1.3$ and $N_{\mathrm{val,exp}} = 14.7$ electrons per Si atom and, for Ne, to $r_{s,\mathrm{exp}} = 1.2$ and $N_{\mathrm{val,exp}} = 18.7$ electrons per Si atom. These are extraordinarily high electron densities per matrix atom, even exceeding the atomic number of the target material, and thus contain no physical meaning. Employing the correct density would require much higher mean charge states than predicted in Ref. [54], which thus is, despite the limitations in the employed modeling, to be expected in the experiment. These quantitative results are consistent with the energy loss ratios reported in Ref. [25], which indicate effective energy dissipation in the target electronic system present only at small impact parameters, particularly for slow heavy ions.

This conclusion is also in accordance with DFT predictions for different ions in Al for a nonhomogeneous electron gas where a significant enhancement of the SCS values for N and Ne ions was observed [64], while minimal effects are produced for H and He ions. Moreover, in a more recent theoretical study [65] for slow ions on TiN employing *ab initio* calculations of the electronic density of TiN, remarkable agreement was found between theoretical results and experimental datasets [66]. The calculations in Ref. [65] again showed that the relative enhancement of the experimental energy loss values with increasing Z_1 beyond predictions by a homogeneous FEG could be described by the effects of high local densities ($r_s = 0.5$–1.5) in the electronic structure of TiN. Explicit calculations for the present systems as well as further experiments assessing the average charge state [67] and the energy loss for different interaction distances, e.g., in different channeling directions, can provide a handle to assess to which extent a locally increased electron density and other more complex excitation processes contribute to the energy deposition.

For the present data, proportionality between electronic SCSs and velocity is observed, while potential deviations at even lower velocities cannot be excluded. Also, for the present approach, no significant effect of the narrow band gap of Si is expected comparing with effects observed for large band gap insulators, with all effects for heavier ions being masked by strong local contributions to the electronic energy loss originating from small-impact parameter collisions. In consequence, from the present results, it can be concluded, that studying effects of details of the target density of states on electronic excitations generated by different ions is only feasible in channeling orientations, where effects of atomic collisions are minimized. Furthermore, the comparison with calculations for a homogeneous FEG is expected to be more accurate in such geometries.

III. SUMMARY AND CONCLUSIONS

We determined the electronic SCSs of Si for H, He, N, and Ne by measuring their energy loss in self-supporting, single-crystalline Si (100) membranes, tilted in (pseudo)random geometries, for energies between 12 to 300 keV. For all ions, the obtained data converged toward velocity proportionality at the lowest studied energies. The obtained results were compared with predictions from SRIM and ESPNN, theoretical predictions from DPASS, measured datasets from the literature, and nonlinear DFT calculations using the literature model reported by Echenique *et al.* [59]. Our results for H ions can be predicted within uncertainties by the DPASS code and SRIM. However, in considering Si as a FEG material for $v/v_0 < 1$, DFT overestimates experimentally deduced values. This observation can be qualitatively explained considering that the small band gap of Si limits the excitations compared with a FEG with the same number of electrons. For He ions, data can be predicted by DFT for velocities below $v/v_0 < 0.7$. This behavior—correct prediction of the specific energy loss of He ions and incorrect of H ions—is inconsistent, especially since, in the calculations, the same energy loss mechanism is responsible for electronic energy deposition for both protons and He ions. Both SRIM and ESPNN underestimate the electronic SCS, while DPASS overestimates it. For N ions, DFT for a uniform FEG predicts lower values by a factor of 50%, while both DPASS and SRIM underestimate the specific energy loss by a factor of $\sim 15\%$. Finally, for Ne ions, DFT for a uniform FEG predicts lower values by a factor of $\sim 80\%$, while SRIM and ESPNN agree with the measured values. Thus, the implemented model based on DFT calculations for a homogeneous FEG, chosen due to its general applicability without a need for further calculations, could not accurately predict the electronic SCS for all ions. It is expected that the displayed discrepancies for heavier ions could be partially eliminated if a nonhomogeneous model for DFT predictions was implemented. However, even though DFT calculations with nonhomogeneous models for a FEG as well as time-dependent DFT calculations could potentially describe the ion-solid interaction in a more accurate way, predicting the specific energy loss more realistically, the fact that they still need to be tailored for each ion-sample system makes their wide implementation up to now impractical.

To summarize, the present results are a clear confirmation that we can accurately predict the energy loss of the interaction of protons with Si; however, for more complex systems, e.g., He, N, or Ne on Si, local and dynamic interactions which contribute to the energy dissipation impede a general quantitative prediction of the electronic energy deposition. Future measurements of the average ion charge state and the energy loss for different geometries and interaction distances could help to disentangle the different contributions to this locally enhanced energy loss.

ACKNOWLEDGMENTS

Accelerator operation was supported by the Swedish Research Council VR-RFI (Contracts No. 2017-00646_9 and No. 2019-00191) and the Swedish Foundation for Strategic Research (Contract No. RIF14-0053).

[1] P. Sigmund, Nucl. Instrum. Methods Phys. B **406**, 391 (2017).
[2] W. H. Bragg and R. Kleeman, The London, London, Edinburgh Dublin Philos. Mag. J. Sci. **10**, 318 (1905).
[3] H. A. Bethe, Ann. Phys. **397**, 325 (1930).
[4] W. H. Barkas, J. N. Dyer, and H. H. Heckman, Phys. Rev. Lett. **11**, 26 (1963).
[5] E. Fermi and E. Teller, Phys. Rev. **72**, 399 (1947).
[6] P. M. Echenique, R. M. Nieminen, and R. H. Ritchie, Solid State Commun. **37**, 779 (1981).
[7] M. Rösler, Nucl. Instrum. Methods Phys. B **69**, 150 (1992).
[8] R. A. Baragiola, C. A. Dukes, and P. Riccardi, Nucl. Instrum. Methods Phys. B **182**, 73 (2001).
[9] J. E. Valdés, J. C. Eckardt, G. H. Lantschner, and N. R. Arista, Nucl. Instrum. Methods Phys. B **73**, 313 (1993).
[10] S. N. Markin, D. Primetzhofer, M. Spitz, and P. Bauer, Phys. Rev. B **80**, 205105 (2009).
[11] D. Roth, B. Bruckner, M. V. Moro, S. Gruber, D. Goebl, J. I. Juaristi, M. Alducin, R. Steinberger, J. Duchoslav, D. Primetzhofer *et al.*, Phys. Rev. Lett **118**, 103401 (2017).
[12] E. E. Quashie, R. Ullah, X. Andrade, and A. A. Correa, Acta Mater. **196**, 576 (2020).
[13] R. Ullah, E. Artacho, and A. A. Correa, Phys. Rev. Lett **121**, 116401 (2018).
[14] S. M. Li, F. Mao, X. D. Zhao, B. S. Li, W. Q. Jin, W. Q. Zuo, F. Wang, and F. S. Zhang, Phys. Rev. B **104**, 214104 (2021).
[15] S. M. Li, F. Mao, X. D. Zhao, W. Q. Jin, W. Q. Zuo, B. S. Li, F. Wang, and F. S. Zhang, Phys. Rev. B **106**, 014103 (2022).
[16] S. N. Markin, D. Primetzhofer, and P. Bauer, Phys. Rev. Lett **103**, 113201 (2009).
[17] M. Draxler, S. P. Chenakin, S. N. Markin, and P. Bauer, Phys. Rev. Lett **95**, 113201 (2005).
[18] J. M. Pruneda, D. Sánchez-Portal, A. Arnau, J. I. Juaristi, and E. Artacho, Phys. Rev. Lett **99**, 235501 (2007).
[19] D. Primetzhofer, S. Rund, D. Roth, D. Goebl, and P. Bauer, Phys. Rev. Lett **107**, 163201 (2011).
[20] M. A. Sortica, V. Paneta, B. Bruckner, S. Lohmann, M. Hans, T. Nyberg, P. Bauer, and D. Primetzhofer, Phys. Rev. A **96**, 032703 (2017).
[21] R. A. Wilhelm and P. L. Grande, Commun. Phys. **2**, 89 (2019).
[22] D. Primetzhofer, D. Goebl, and P. Bauer, Nucl. Instrum. Methods Phys. B **317**, 8 (2013).
[23] S. Creutzburg, A. Niggas, D. Weichselbaum, P. L. Grande, F. Aumayr, and R. A. Wilhelm, Phys. Rev. A **104**, 042806 (2021).
[24] S. Lohmann and D. Primetzhofer, Phys. Rev. Lett **124**, 096601 (2020).
[25] S. Lohmann, R. Holeňák, and D. Primetzhofer, Phys. Rev. A **102**, 062803 (2020).
[26] E. Ntemou, R. Holeňák, and D. Primetzhofer, Radiat. Phys. Chem. **194**, 110033 (2022).
[27] A. Lim, W. M. C. Foulkes, A. P. Horsfield, D. R. Mason, A. Schleife, E. W. Draeger, and A. A. Correa, Phys. Rev. Lett. **116**, 043201 (2016).
[28] B. Bruckner, P. M. Wolf, P. Bauer, and D. Primetzhofer, Nucl. Instrum. Methods Phys. B **489**, 82 (2021).
[29] A. Schinner, V. I. Shulga, and P. Sigmund, J. Appl. Phys. **129**, 185304 (2021).
[30] P. Sigmund and A. Schinner, Eur. Phys. J. D **12**, 425 (2000).
[31] A. Schinner and P. Sigmund, Nucl. Instrum. Methods Phys. B **460**, 19 (2019).
[32] A. Schinner and P. Sigmund, DPASS program, https://www.sdu.dk/en/dpass.
[33] F. Bivort Haiek, A. M. P. Mendez, C. C. Montanari, and D. M. Mitnik, arXiv:2210.10950.
[34] https://github.com/ale-mendez/ESPNN.
[35] M. Linnarsson, A. Hallen, K. J. Astrom, D. Primetzhofer, S. Legendre, and G. Possnert, Rev. Sci. Instrum. **83**, 095107 (2012).
[36] M. S. Sortica, M. K. Linnarsson, D. Wessman, S. Lohmann, and D. Primetzhofer, Nucl. Instrum. Methods Phys. B **463**, 16 (2020).
[37] https://www.roentdek.com/.
[38] H. Winter and H. P. Winter, Europhys. Lett. **62**, 739 (2003).
[39] https://www.norcada.com/.
[40] J. F. Ziegler, M. D. Ziegler, and J. P. Biersack, Nucl. Instrum. Methods Phys. B **268**, 1818 (2010).
[41] S. Lohmann, R. Holeňák, P. L. Grande, and D. Primetzhofer, Phys. Rev. B **107**, 085110 (2023).
[42] J. P. Biersack, E. Steinbauer, and P. Bauer, Nucl. Instrum. Methods Phys. B **61**, 77 (1991).
[43] J. F. Ziegler, J. P. Biersack, and U. Littmark, *The Stopping and Range of Ions in Solids* (Pergamon Press, New York, 1983), Vol. 1.
[44] G. Moliere, Z. Naturforsch. A **2**, 133 (1947).
[45] T. T. Tran, L. Jablonka, B. Bruckner, S. Rund, D. Roth, M. A. Sortica, P. Bauer, Z. Zhang, and D. Primetzhofer, Phys. Rev. A **100**, 032705 (2019).
[46] M. Brocklebank, S. N. Dedyulin, and L. V. Goncharova, Eur. Phys. J. D **70**, 248 (2016).
[47] A. Ikeda, K. Sumitomo, T. Nishioka, and Y. Kido, Nucl. Instrum. Methods Phys. B **115**, 34 (1996).
[48] G. Konac, S. Kalbitzer, Ch. Klatt, D. Niemann, and R. Stoll, Nucl. Instrum. Methods Phys. B **136**, 159 (1998).
[49] G. Hobler, K. K. Bourdelle, and T. Akatsu, Nucl. Instrum. Methods Phys. B **242**, 617 (2006).
[50] M. Famá, G. H. Lantschner, J. C. Eckardt, N. R. Arista, J. E. Gayone, E. Sanchez, and F. Lovey, Nucl. Instrum. Methods Phys. B **193**, 91 (2002).
[51] D. Niemann, G. Konac, and S. Kalbitzer, Nucl. Instrum. Methods Phys. B **118**, 11 (1996).
[52] M. Mery, J. D. Uribe, M. Flores, N. R. Arista, V. A. Esaulov, and J. E. Valdés, Radiat. Eff. Defects Solids **176**, 73 (2021).
[53] https://physics.nist.gov/PhysRefData/Star/Text/programs.html.
[54] J. D. Pearce and R. R. Hart, J. Appl. Phys. **52**, 5056 (1981).
[55] N. P. Barradas, E. Alves, Z. Siketić, and I. Bogdanović Radović, AIP Conf. Proc. **1099**, 331 (2009).
[56] D. C. Santry and R. D. Werner, Nucl. Instrum. Methods Phys. B **53**, 7 (1991).
[57] H. Grahmann and S. Kalbitzer, Nucl. Instrum. Methods **132**, 119 (1976).
[58] I. Hoffman, E. Jager, and U. Muller-Jahreis, Radiat. Eff. **31**, 57 (1976).
[59] P. M. Echenique, F. Flores, and R. H. Ritchie, Solid State Phys. **43**, 229 (1990).
[60] D. Isaacson, *Compilation of r_s values, Doc. No. 02698, Radiation and Solid State Laboratory* (New York University, 1975).
[61] A. Mann and W. Brandt, Phys. Rev. B **24**, 4999 (1981).
[62] H. H. Brongersma, M. Draxler, M. de Ridder, and P. Bauer, Surf. Sci. Rep. **62**, 63 (2007).
[63] D. Runco and P. Riccardi, Phys. Rev. A **104**, 042810 (2021).

[64] J. Calera-Rubio, A. Gras-Marti, and N. R. Arista, Nucl. Instrum. Methods Phys. B **93**, 137 (1994).

[65] F. Matias, P. L. Grande, M. Vos, P. Koval, N. E. Koval, and N. R. Arista, Phys. Rev. A **100**, 030701(R) (2019).

[66] M. A. Sortica, V. Paneta, B. Bruckner, S. Lohmnann, T. Nyberg, P. Bauer, and D. Primetzhofer, Sci. Rep. **9**, 176 (2019).

[67] R. Holeňák, S. Lohmann, F. Sekula, and D. Primetzhofer, Vacuum **185**, 109988 (2021).